

Comparison of KP1019 and NAMI-A in tumour-mimetic environments – electronic supplementary information

Gemma K. Gransbury,^{a,§} Peter Kappen,^b Chris J. Glover,^b James N. Hughes,^c Aviva Levina,^d Peter A. Lay,^d Ian F. Musgrave,^e and Hugh H. Harris*^a

^aDepartment of Chemistry, ^cDepartment of Molecular and Cellular Biology, ^eSchool of Medical Sciences, The University of Adelaide, SA 5005, Australia

^bAustralian Synchrotron, Clayton, VIC 3168, Australia

^dSchool of Chemistry, The University of Sydney, NSW 2006, Australia

Control spheroids for hypoxia assay

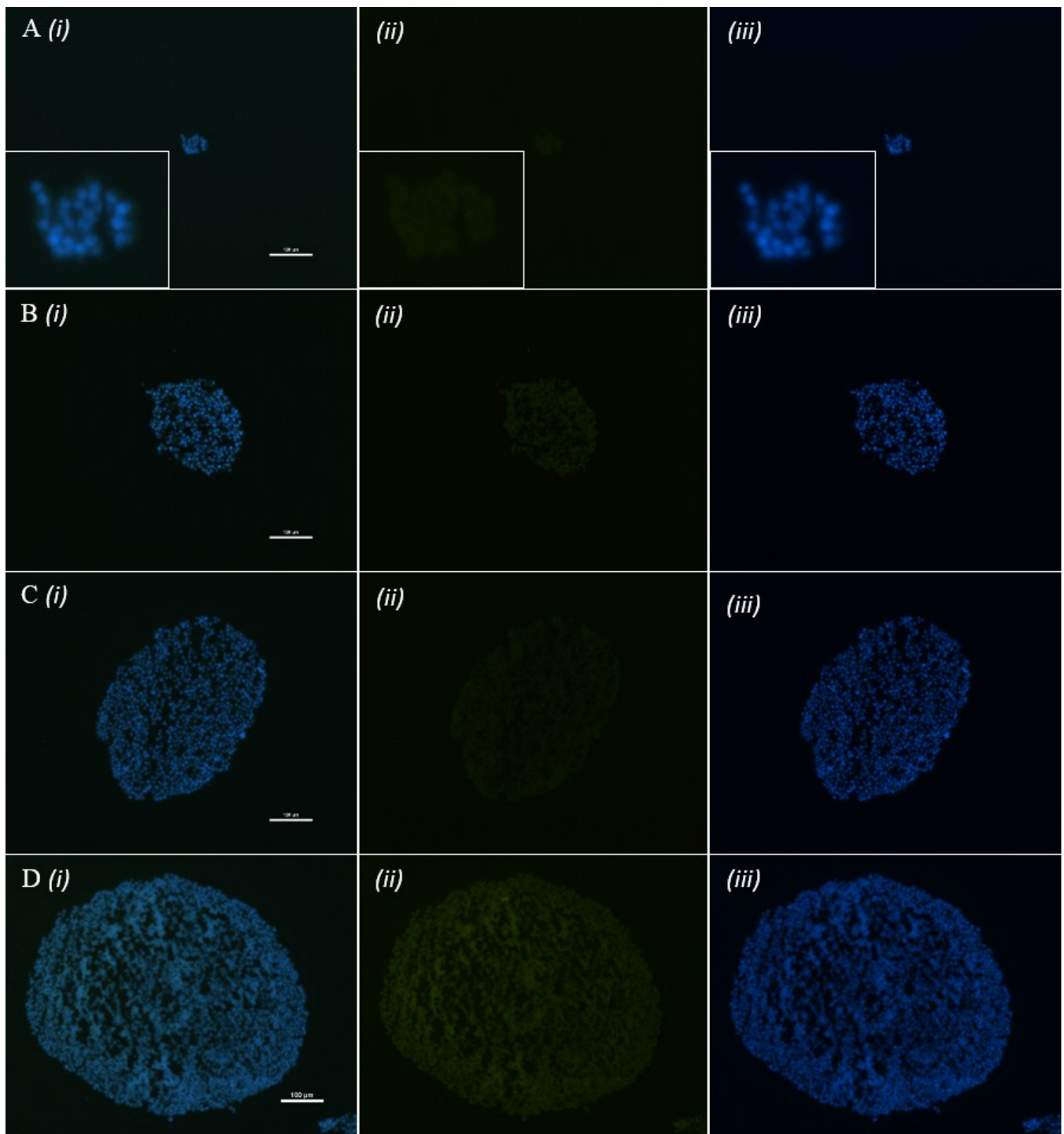


Figure S1: Representative control spheroids from the following size groups: (A) 50-150 μm, (B) 200-300 μm, (C) 300-450 μm and (D) 700-800 μm, treated with Hypoxyprobe-1 MAb1 and imaged with green fluorescent donkey anti-mouse antibody. Overlaid image (i) of background green stain (ii) and nuclear stain (iii); scale bars represent 100 μm.

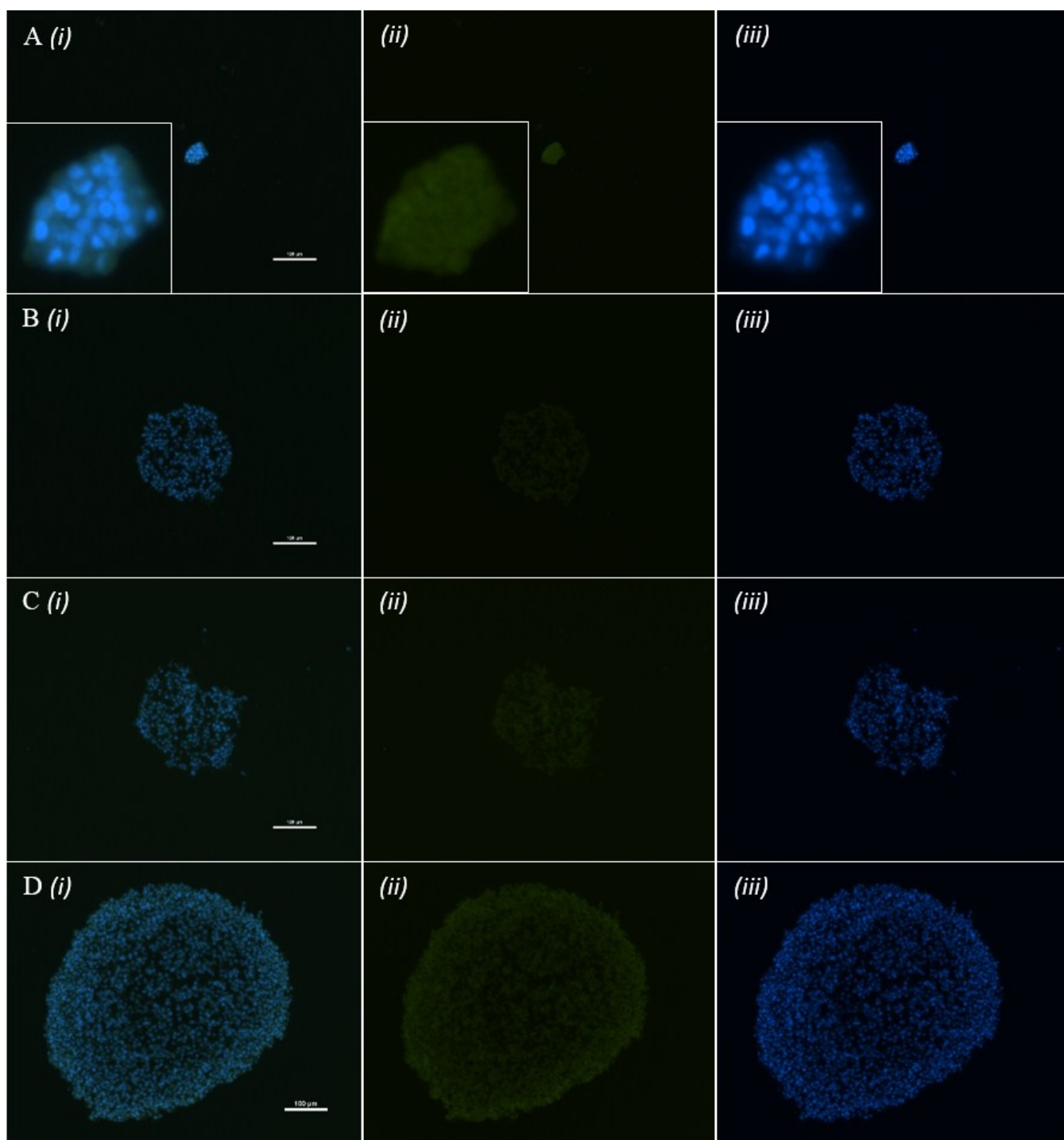


Figure S2: Representative control spheroids from the following size groups: (A) 50-150 μm, (B) 200-300 μm, (C) 300-450 μm and (D) 700-800 μm, untreated and imaged with green fluorescent donkey anti-mouse antibody. Overlaid image (i) of background green stain (ii) and nuclear stain (iii); scale bars represent 100 μm.

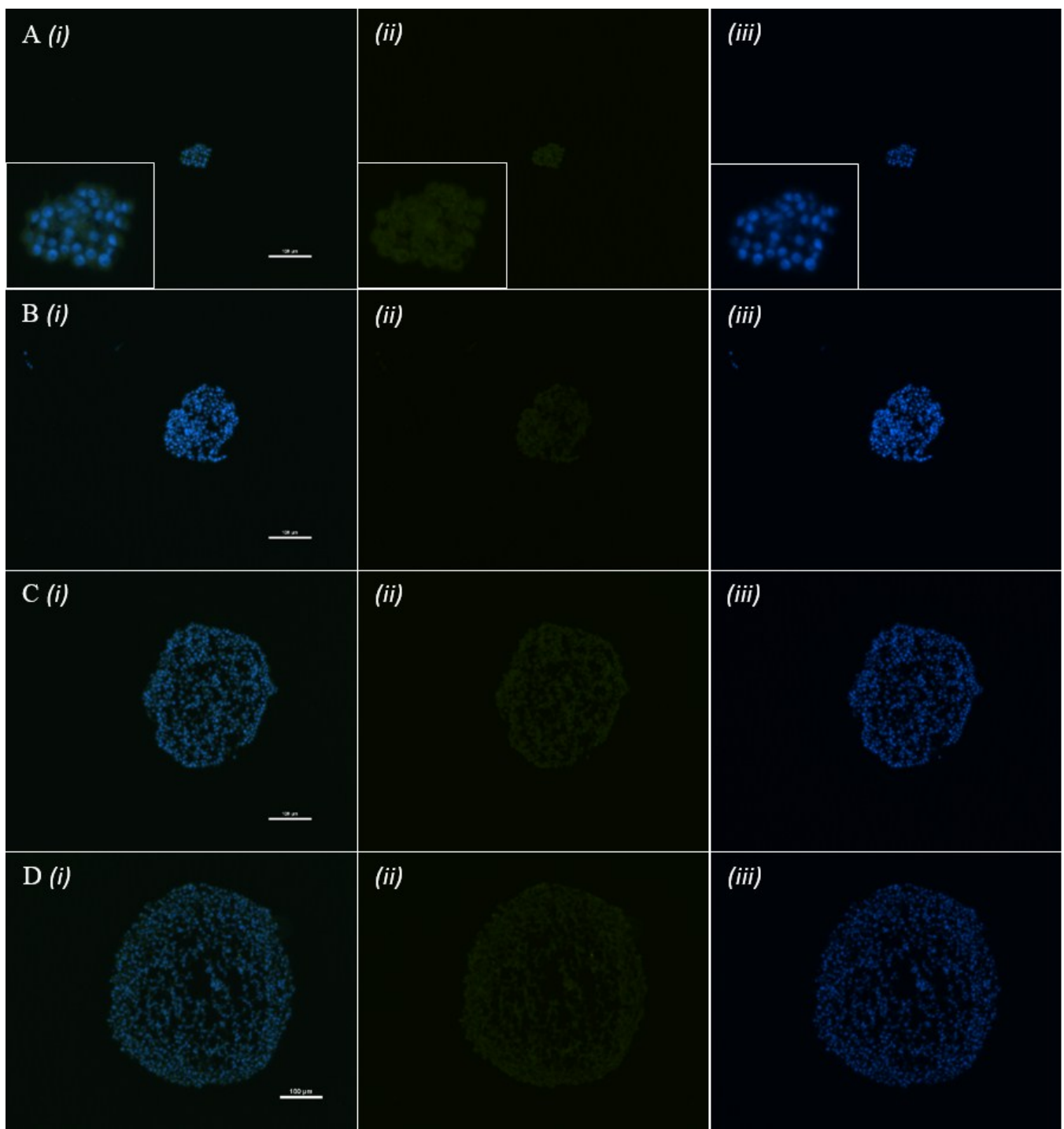


Figure S3: Representative control spheroids from the following size groups: (A) 50-150 μm , (B) 200-300 μm , (C) 300-450 μm and (D) 700-800 μm , treated with pimonidazole hydrochloride and imaged with green fluorescent donkey anti-mouse antibody. Overlaid image (i) of background green stain (ii) and nuclear stain (iii); scale bars represent 100 μm .

Alternative Edge Energy Calculation

An alternative method to calculate the Ru K-edge energy used the first peak of the derivative spectrum. A cubic function was modelled to the spectrum in 3 eV ranges about each point, and used to calculate the derivative spectra. The error was given by the energy step over the edge region (0.4 eV) combined with three times the standard deviation of Ru⁰ foil edge calibration energies on each side.

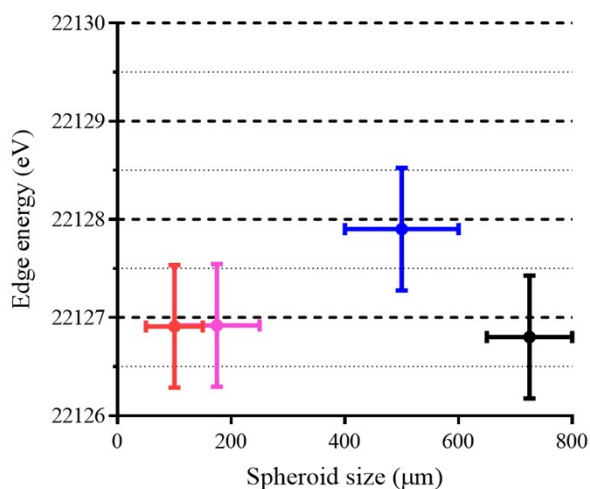


Figure S5: Ru K-edge energies of spheroids treated with 500 μM NAMI-A as a function of spheroid size.

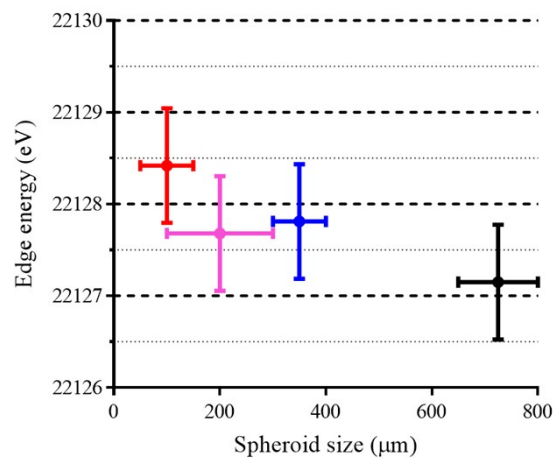


Figure S6: Ru K-edge energies of spheroids treated with 500 μM KP1019 as a function of spheroid size.

Fitting background for LA-ICP-MS

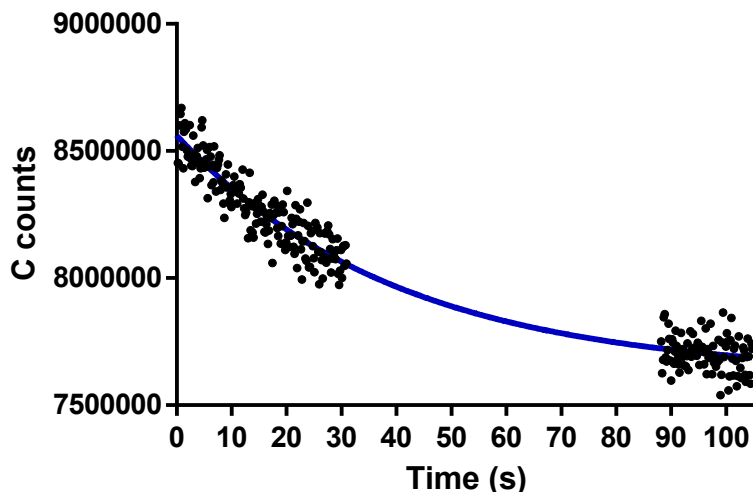


Figure S7: Example of fitting of first order decay to background ^{12}C signal: $y = (9.42 \text{ \AA} - 10^5)e^{-0.02495x} + 7.619 \text{ \AA} - 10^6$

EXAFS

EXAFS analyses of NAMI-A, monoculture cells treated with NAMI-A at 200 μM for 24 h and various size spheroids treated with 500 μM NAMI-A for 24 h are presented in Table S1. The fit errors were much larger for biological samples indicating that Ru was present in low concentrations as a complicated mixture of species, which could not be modelled accurately with low signal-to-noise ratios. In a number of fitted models, the total first shell coordination number was less than six. Such a situation is chemically unlikely for Ru, and the fact that such models are often better fits for the data indicates that more complex average coordination environments would have to be considered to yield satisfactory fits with a total coordination number of six. These environments will presumably contain a complex mixture of scattering interactions across a range of bond lengths resulting from the mixture of species that are likely to be present in the biological samples, but would require the collection of higher quality data to fit in a meaningful way. The data analysis utilized a conservative many body amplitude reduction factor (S_0^2) of 0.9 – although this was not rigorously parameterized against a model compound set we note that using a higher value would only lead to even smaller fitted total coordination numbers for this dataset.

Table S1: Parameters for EXAFS fits of NAMI-A standard, monoculture cells and spheroid samples treated with NAMI-A.^a

Sample	Concentration of NAMI-A (μM)	<i>k</i> -range (Å ⁻¹)	Scatterer	Coordination Number (<i>N</i> _{fix})	Interatomic distance (<i>R</i> , Å)	Debye-Waller factor (σ ² , Å ²)	-Δ <i>E</i> ₀ (eV)	Fit error ^b		
NAMI-A	N/A	14	N/O	1	2.090 (9)	0.0014 (7)	-7.5 (0.4)	0.2820		
			S/Cl	5	2.355 (2)	0.00340 (9)				
Monoculture	200	12	N/O	4	2.06 (1)	0.005 (1)	-15.5 (1.7)	0.5402		
			S/Cl	2	2.25 (1)	0.006 (1)				
			N/O	3	2.05 (1)	0.006 (2)			-19.0 (2.0)	0.5400
			S/Cl	3	2.23 (1)	0.0076 (8)				
Small spheroids	500	12	N/O	4	2.071 (5)	0.0011 (4)	-11.4 (1.2)	0.5229		
			S/Cl	1	2.30 (2)	0.005 (1)				
			N/O	5	2.081 (5)	0.0027 (5)			-11.2 (1.2)	0.5268
			S/Cl	1	2.27 (3)	0.010(3)				
			N/O	4	2.074 (5)	0.0017 (5)			-13.2 (1.4)	0.5236
			S/Cl	2	2.26 (2)	0.012 (2)				
Medium spheroids	500	12	N/O	5	2.098 (6)	0.0025 ^c	-12.1 (1.4)	0.6245		
			S/Cl	1	2.185 (8)	0.0025 ^c				
			N/O	5	2.101 (6)	0.0025 ^c			-11.8 (1.3)	0.6102
			S/Cl	1	2.184 (8)	0.0025 ^c				
Medium-large spheroids	500	12	Ru	0.5	2.79 (1)	0.003 (1)	-8.4 (1.1)	0.5883		
			N/O	5	2.107 (6)	0.0033 (6)				
			S/Cl	1	2.20 (2)	0.008				
			N/O	5	2.101 (5)	0.0028 (3)			-6.3 (0.9)	0.6082
Large spheroids	500	14	N/O	4	2.088 (4)	0.0044 (4)	-13.0 (1.0)	0.4630		
			S/Cl	2	2.26 (1)	0.0099 (9)				

^a A scale factor (*S*⁰²) of 0.9 was used for all fits and Δ*E*₀ = *E*₀ - 22118 eV, where *E*₀ is the threshold energy. Values in parentheses are the estimated standard deviation derived from the diagonal elements of the covariance matrix and are a measure of precision. More realistic error analysis can be found in the following.^{1,2} The fit-error is defined as $[\sum k^6(\chi_{\text{exp}} - \chi_{\text{calc}})^2 / \sum k^6 \chi_{\text{exp}}^2]^{1/2}$. ^b Fit errors can only be directly compared between fits to the same data and not across sample. ^c must be constrained to a chemically reasonable number to obtain a good fit.

The NAMI-A standard was fitted with 1 N and 5 Cl; the Cl represented Cl and S backscatterers, which cannot be distinguished by EXAFS fitting. The N scatterer was difficult to fit accurately as the EXAFS were dominated by the 5 heavy-element scatterers. Bond lengths in the crystal structure of the sodium salt of the NAMI-A anion co-crystallised with water and acetone³ were used to give initial conditions for the EXAFS fit. The final bond lengths of 2.355 (2) Å for Ru-S/Cl and 2.090 (9) Å for Ru-N/O gave close agreement with the crystal parameters: 2.296 Å for Ru-S, 2.323-2.359 Å for Ru-Cl and 2.081 Å for Ru-N. The final EXAFS fit for NAMI-A is shown in Figure S8 (A).

NAMI-A treated spheroids of all sizes as well as treated monoculture cells had very similar EXAFS, as indicated by *k*³-weighted EXAFS in *k*-space, Fourier transforms (FTs) in *R*-space and similar ratios of O/N and S/Cl scatterers, varying from 5:1 to 3:3 (see Figure S8 and Table S1). The Ru-O/N and Ru-S/Cl scattering contributions were poorly resolved but the presence of Ru-S/Cl interactions was validated by significant residual peaks at 2.4 Å in the FT when only O/N scatterers were considered. As the samples are complex biological mixtures of Ru species, a distribution of Ru-O/N and Ru-S/Cl bond lengths in the sample is expected and may contribute to poor peak resolution. Modelled Ru-O/N bonds vary from 2.05-2.11 Å while Ru-S/Cl bond lengths were found over a large range of 2.18-2.30 Å. Increased S/Cl coordination resulted in shorter Ru-S/Cl bond lengths and increased Debye-Waller factors. Lower fit errors were observed with increased Ru-S/Cl contributions; however, a strong correlation between the number of coordinated S/Cl ligands and Δ*E*₀ reduced confidence in the fitting results.

The reduced contribution of heavy Cl/S scatters in treated spheroid spectra relative to the NAMI-A standard is consistent with substitution of the most labile ligands. The chlorido ligands are expected to be most labile and other groups may also be substituted, albeit more slowly.^{4,5} The dominance of O/N donors is thought to arise from aquation of NAMI-A and NAMI-A – BSA adducts. NAMI-A binds to BSA with a first coordination shell of 60% N and 40% O while remaining in the Ru^{III} oxidation state.^{6,7} These I-A – protein adducts may form in cell culture media or with cell membrane proteins.⁷ In addition, there is a small but significant fraction of Ru binding to sulfur residues of proteins. Significant Ru-S binding contributions (62%) have been reported in previous XAS studies of NAMI-A-treated HepG2 monoculture cells based on linear combinations of standard Ru complex spectra.⁵

Peaks at high *R* arise from second shell and multiple-scattering interactions,¹ which cannot necessarily be fit accurately for spectra with low signal-to-noise ratios and where a complicated mixture of Ru complexes is present, as expected in biological systems. There was limited evidence for a small fraction of Ru-Ru interactions in the treated spheroid and cell spectra,

observed around 2.8 Å in medium spheroids treated with NAMI-A, and at around 3.1 Å in medium-large spheroids treated with NAMI-A (see Table S1). However, while polynuclear ruthenium complexes are not unprecedented in biological chemistry, their presence cannot be confirmed without full consideration of multiple-scattering interactions.⁵

Residual peaks below 1.5 Å were at chemically unreasonable bond lengths may correspond to series truncation artefact or 'ringing' peaks derived from performing a FT over a finite region of k -space, or from atomic X-ray absorption fine structure (AXAFS) contributions.¹ The residual at low k for treated cell and spheroid spectra indicated that not all components of the spectra were well fit. This was attributed to the range of Ru-O/N and Ru-S/Cl bond lengths discussed above, limitations of FEFF8 calculations at low k , ignorance of multiple-scattering paths and possible AXAFS contributions.

The EXAFS fitting was insufficient to unambiguously assign the coordination sphere of Ru in the biological samples treated with NAMI-A, for the reasons stated above. However, it was concluded that both Ru-O/N and Ru-S/Cl scatterers were present in all spheroid and monoculture cell samples, in ratios between 5:1 and 3:3. A significant difference between the NAMI-A standard spectra and the treated samples was observed, indicating the chlorido and/or the DMSO ligands were exchanged for increased Ru-O/N coordination. There was also limited evidence of Ru-Ru interactions in the treated medium and medium-large spheroid spectra. As hypoxia levels increase, there was no conclusive evidence of changing Ru coordination environment in NAMI-A treated samples.

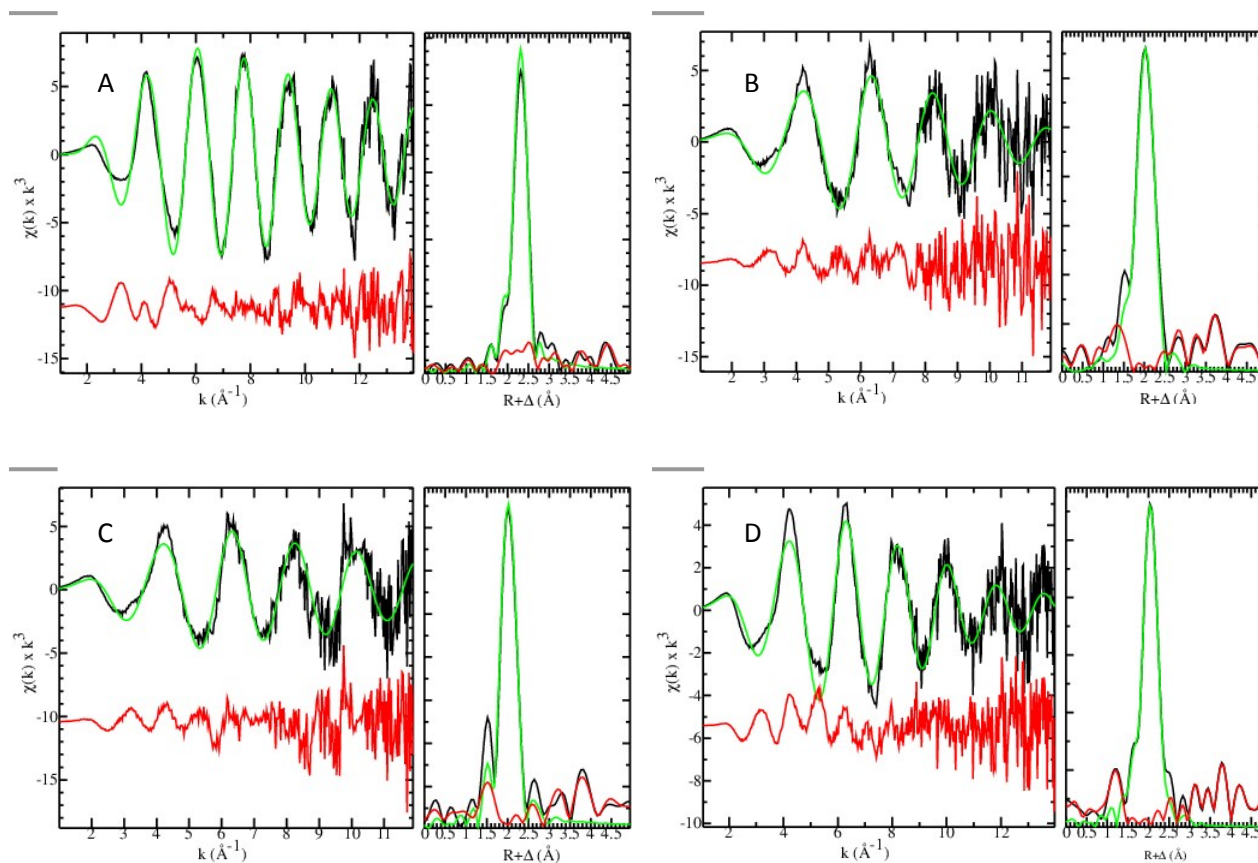


Figure S8: EXAFS fits of NAMI-A standard (A), of monoculture cells treated with 200 μM NAMI-A (B), small spheroids treated with 500 μM NAMI-A (C) and large spheroids treated with 500 μM NAMI-A (D). On the left is the k^2 -weighted EXAFS in k -space and on the right is the phase-corrected Fourier transform. Raw data (black), calculated fit (green) and residual of the fits (red) are shown. Parameters of the fits are indicated in bold typeface in Table S1.

EXAFS analyses of KP1019, monoculture cells treated with KP1019 at 200 μM for 24 h and various size spheroids treated with 500 μM NAMI-A for 24 h are presented in Table S2. As for NAMI-A EXAFS, the large fit errors for the biological samples indicated that Ru was present in low concentrations as a complicated mixture of species which could not be modelled accurately with low signal-to-noise ratios.

Bond distances from the crystal structure of the KP1019 anion with an (indazole)₂H⁺ cation⁸ were used to give initial conditions for EXAFS fitting. The final bond length of 2.361 (2) Å for Ru-Cl was within error of the crystal structure bond length, 2.362 Å. The Ru-N distance was fit to 2.15 (2) Å which was somewhat larger than the bond length of 2.062 Å in the crystal structure. The

bond length discrepancy arose from the EXAFS being dominated by heavy Cl scatterers, limiting the accuracy of fitting parameters for N. The best fit for the KP1019 standard is shown in Figure S9 (A).

Table S2: Parameters for EXAFS fits of KP1019 standard, monoculture cells and spheroid samples treated with KP1019.^a

Sample	Concentration of KP1019 (μM)	k-range (\AA^{-1})	Scatterer	Coordination Number (N_{fix})	Interatomic distance (R , \AA)	Debye-Waller factor (σ^2 , \AA^2)	$-\Delta E_0$ (eV)	Fit-error ^b
KP1019	N/A	14	N/O	2	2.15 (2)	0.011 (2)	-6.7 (0.6)	0.2932
			S/Cl	4	2.361 (2)	0.00255 (9)		
Monoculture cells	200	14	N/O	4	2.076 (2)	0.0014 (2)	-9.7 (0.6)	0.4103
			Ru	0.5	3.194 (5)	0.0023 (4)		
			N/O	6	2.077 (2)	0.0036 (2)	-9.5 (0.6)	0.4590
			Ru	0.5	3.193 (5)	0.0026 (4)		
			N/O	4	2.072 (2)	0.0017 (2)	-12.3 (0.8)	0.3976
			S/Cl	1	2.20 (2)	0.014 (3)		
Small spheroids	500	12	N/O	3.5	2.061 (5)	0.0021 (4)	-12.1 (1.1)	0.4636
			S/Cl	1	2.26 (2)	0.009 (2)		
			Ru	1.5	3.193 (9)	0.0081 (7)		
			N/O	4.5	2.070 (3)	0.0028 (2)	-10.4 (0.7)	0.4746
			Ru	3	3.204 (8)	0.0116 (8)		
			N/O	4.5	2.085 (3)	0.0019 (2)	-9.0 (0.7)	0.4650
Medium spheroids	500	12	N/O	4	2.078 (6)	0.0027 (3)	-11.5 (0.8)	0.4556
			S/Cl	0.5	2.22 (1)	0.0025^c		
			Ru	1.5	3.20 (1)	0.010 (1)		
			N/O	5	2.07 (1)	0.0085 (7)	-14.7 (1.2)	0.4454
			S/Cl	1	2.209 (5)	0.0013 ^c		
			Ru	1.5	3.19 (1)	0.010 (1)		
Medium-large spheroids	500	14	N/O	4.5	2.067 (3)	0.0021 (2)	-11.0 (0.9)	0.5733
			Ru	0.5	2.866 (7)	0.0029 (5)		
			N/O	6	2.071 (4)	0.0038 (2)	-10.6 (0.9)	0.5898
			Ru	0.5	2.870 (6)	0.0025 (5)		
			N/O	4.5	2.064 (3)	0.0014 (2)	-10.6 (0.9)	0.5581
			S/Cl	0.5	2.33 (1)	0.007 (1)		
Large spheroids	500	14	N/O	4	2.082 (3)	0.0021 (2)	-10.3 (0.7)	0.4325
			S/Cl	1	2.32 (7)	0.0047 (7)		
			N/O	3	2.075 (3)	0.0010 (2)	-11.8 (0.8)	0.4306
			S/Cl	1.5	2.298 (7)	0.0061 (6)		
			N/O	3	2.075 (3)	0.0014 (2)	-12.9 (0.9)	0.4312
			S/Cl	2	2.285 (8)	0.0086 (6)		
N/O	5	2.096 (3)	0.0033 (2)	-8.9 (0.6)	0.4749			
N/O	6	2.098 (3)	0.0044 (2)	-8.7 (0.6)	0.4828			

^a The best fits to each spectra are highlighted in bold. A scale factor (S_0^2) of 0.9 was used for all fits and $\Delta E_0 = E_0 - 22118$ eV, where E_0 is the threshold energy. Values in parentheses are the estimated standard deviation derived from the diagonal elements of the covariance matrix and are a measure of precision. More realistic error analysis can be found in the following.^{1,2} The fit-error is defined as $[\sum k^6(\chi_{\text{exp}} - \chi_{\text{calc}})^2 / \sum k^6 \chi_{\text{exp}}^2]^{1/2}$. ^b Fit errors can only be directly compared between fits to the same data and not across sample. ^c Must be constrained to a chemically reasonable number to obtain a good fit.

The EXAFS analysis of KP1019-treated monoculture cells and spheroids yielded results that were significantly different from that of the spheroids treated with NAMI-A; Ru-S/Cl scattering contributions were generally smaller, strong evidence of Ru-Ru scattering was observed and fits changed with spheroid size. EXAFS of treated monoculture cells and spheroids were dominated by Ru-N/O scatterers at 2.06-2.08 \AA with coordination numbers between 3.5 and 4.5. The fits in almost every case were best for a total coordination number of Ru-O/N and Ru-S/Cl contributions of less than six, as indicated by comparisons to six-coordinate models (see Table S2). The Ru-O/N bond distance was sensitive to coordination number of S/Cl, and so was not a good indication of potential reduction of Ru^{III} to Ru^{II}.

The evidence of Ru-S/Cl interactions in EXAFS of monoculture cells and small, medium and medium-large spheroids treated with KP1019 was much weaker than for NAMI-A-treated monoculture cells and spheroids. EXAFS modelling of KP1019-treated

monoculture cells and medium-large spheroids with only Ru-N/O and Ru-Ru scattering contributions did not result in significant residual peaks around 2.3 Å. Consideration of Ru-S/Cl interactions improved the fit error, as expected for introducing three new parameters; however, the residual under the main peak increased and resulted in chemically unreasonable Debye-Waller factors for the Ru-N/O interaction. The EXAFS of KP1019-treated monoculture cells and medium-large spheroids therefore showed no strong evidence of Ru-S/Cl contributions.

EXAFS fits of small and medium KP1019-treated spheroid spectra with only Ru-N/O and Ru-Ru interactions indicated a very small residual peak around 2.3 Å suggesting the presence of a small fraction of Ru-S/Cl species. Accurate modelling of Ru-S/Cl interactions in these spectra was complicated by lower bond length resolution and resulted in chemically unreasonable Ru-S/Cl Debye-Waller factors if not restrained. The evidence of Ru-S/Cl interactions at 2.20-2.26 Å in small- and medium-sized KP1019-treated spheroids is weak as the bond distances are short and the residual peak may be a result of a distribution of Ru-N/O bond lengths which was unable to be modelled accurately.

Ru-S/Cl interactions are present in the EXAFS of large spheroids treated with KP1019 as evidenced by a large residual around 2.4 Å when only Ru-N/O interactions are considered; a Ru-S bond length of 2.32 Å, close to 2.296 Å as observed in the NAMI-A crystal structure and chemically reasonable Debye-Waller factors for Ru-S/Cl and Ru-N/O scattering interactions. Models including only Ru-O/N scatterers were poor, as indicated by high fit errors (see Table S2). The most reasonable fit parameters for EXAFS of large KP1019-treated spheroids were obtained for 4 N and 1 S scatterers. A higher S coordination number resulted in lower fit errors but less chemically reasonable values of the Debye-Waller factor and ΔE_0 (see Table S2). The fraction of Ru-S/Cl is less than reported for KP1019-treated liver cancer monoculture cells (49%).⁵ It is unlikely that Ru would form a complex with a coordination number less than six, as both Ru^{II} and Ru^{III} form octahedral complexes. The lower total coordination number may indicate lower symmetry Ru centres and some EXAFS cancellation.⁹

Ru-Ru interactions have been observed in literature at 3.15 (2) Å ($N = 1.6$) for the decomposition of KP1019 in neutral aqueous buffered solution.⁵ A linear combination of standard XANES spectra has previously indicated that the decomposition product of KP1019 contained a high proportion of Ru^{IV}O₂ (32 %) while a dark precipitate was observed. Levina and co-workers concluded that polynuclear and partially oxidized Ru^{III/IV}_xO_y clusters were formed in aqueous solution.⁵ In their work, a green discoloration was observed for KP1019 in media after ~15 min and cell and spheroid samples retained this discoloration. In this work, a dark green precipitate formed for concentrations > 1 mM in cell culture media.

Ru-Ru interactions were characterized by a broad, low magnitude peak around $k = 8.5 \text{ \AA}^{-1}$, as seen in the EXAFS of treated monoculture cells (see Figure S9 (B)). There was strong evidence for Ru-Ru interactions in this sample as the peak at 3.194 (5) Å fit closely with the FT. Evidence for the presence of Ru-Ru interactions in treated small spheroids was limited by data collected to only $k = 12 \text{ \AA}^{-1}$ and the low signal-to-noise ratio. The peak at 3.20 (1) Å did not fit the FT well; however, the broad, lower intensity peak at $k = 8.5 \text{ \AA}^{-1}$ and poor fit of Ru-O/N and Ru-S/Cl alone indicated that Ru-Ru was present in KP1019-treated small spheroids (see Figure S9 (C)). Similar evidence of Ru-Ru scattering contributions was observed in EXAFS of medium KP1019-treated spheroids. The coordination number of Ru-Ru interactions for treated small and medium spheroids was imprecise as fitting the Ru-Ru peak attempted to fit the multiple-scattering peaks on either side. This resulted in large coordination numbers and Debye-Waller factors.

EXAFS from medium-large spheroids were fitted with Ru-Ru interactions at ~2.87 Å instead of ~3.20 Å; a viable Ru-Ru bond length observed in complexes in the CSD. This improved the fit in k -space and R -space with the high resolution $k_{max} = 14 \text{ \AA}^{-1}$ data (see Figure S10). Ru-Ru interactions in medium-large KP1019-treated spheroids were confirmed by a broad, low magnitude peak around $k = 8.5 \text{ \AA}^{-1}$ and an increase in the oscillation amplitude above $k = 12 \text{ \AA}^{-1}$. The presence of two Ru-Ru bond distances across the spheroid samples may be a result of different biochemical make-up, including oxygen concentration, pH and ruthenium concentration in different regions. As discussed above, Ru-Ru interactions may be a result of Ru^{III/IV}_xO_y cluster formation.

Large treated spheroids showed no evidence of Ru-Ru interactions, indicated by a narrow peak at $k = 8 \text{ \AA}^{-1}$ and the lack of significant FT peaks above 2.5 Å. This suggested that high levels of hypoxia, and necrosis, either prevent the formation of polynuclear Ru species such as the proposed Ru^{III/IV}_xO_y clusters or decomposed them into mononuclear species.

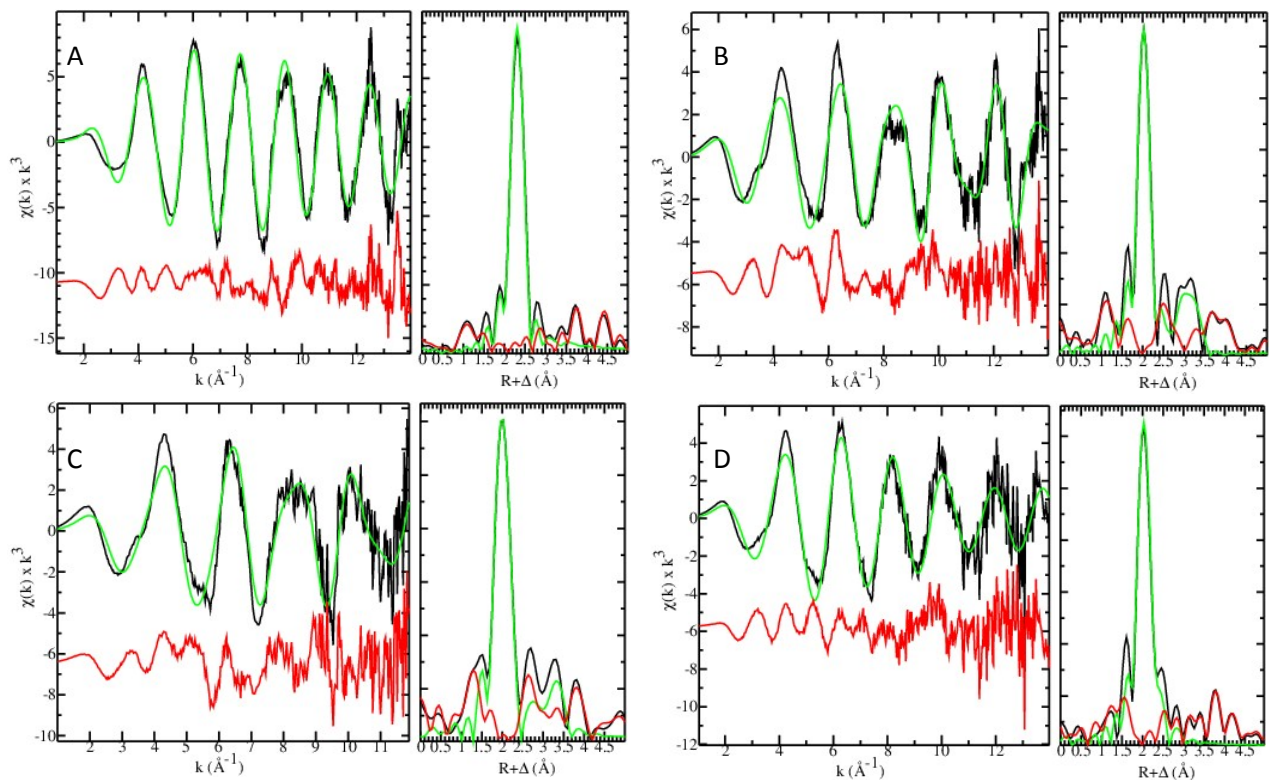


Figure S9. EXAFS fits of KP1019 standard (A), of monoculture cells treated with 200 μM KP1019 (B), small spheroids treated with 500 μM KP1019 (C) and large spheroids treated with 500 μM KP1019 (D). On the left is the k^3 -weighted EXAFS in k -space and on the right is the phase corrected Fourier transform. Raw data (black), calculated fit (green) and residual of the fits (red) are shown. Parameters of the fits are highlighted in bold in Table S2.

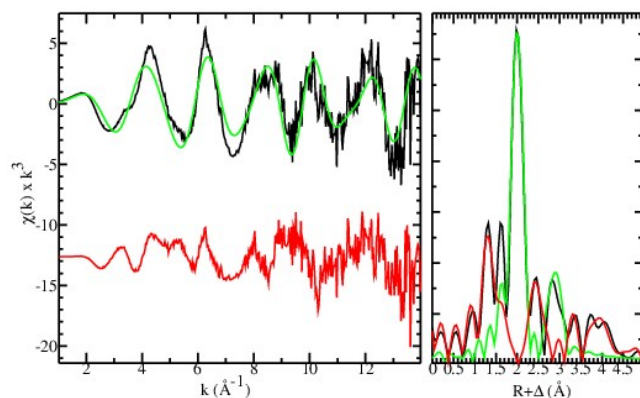


Figure S10. EXAFS fit of medium-large spheroids treated with 500 μM KP1019 with Ru-Ru interactions as 2.866 \AA . On the left is the k^3 -weighted EXAFS in k -space and on the right is the phase corrected Fourier transform. Raw data (black), calculated fit (green) and residual of the fits (red) are shown. Parameters of the fit are shown in Table S2.

References

1. A. Levina, R. S. Armstrong and P. A. Lay, *Coord. Chem. Rev.*, 2005, **249**, 141-160.
2. A. M. Rich, R. S. Armstrong, P. J. Ellis, H. C. Freeman and P. A. Lay, *Inorg. Chem.*, 1998, **37**, 5743-5753.
3. E. Alessio, G. Balducci, A. Lutman, G. Mestroni, M. Calligaris and W. M. Attia, *Inorg. Chim. Acta*, 1993, **203**, 205-217.
4. M. I. Webb and C. J. Walsby, *Metallomics*, 2013, **5**, 1624-1633.
5. A. Levina, J. B. Aitken, Y. Y. Gwee, Z. J. Lim, M. Liu, A. M. Singharay, P. F. Wong and P. A. Lay, *Chem. - Eur. J.*, 2013, **19**, 3609-3619.
6. I. Ascone, L. Messori, A. Casini, C. Gabbiani, A. Balerna, F. Dell'Unto and A. Congiu Castellano, *Inorg. Chem.*, 2008, **47**, 8629-8634.
7. M. Liu, Z. J. Lim, Y. Y. Gwee, A. Levina and P. A. Lay, *Angew. Chem., Int. Ed.*, 2010, **49**, 1661-1664.
8. E. Reisner, V. B. Arion, A. Eichinger, N. Kandler, G. Giester, A. J. L. Pombeiro and B. K. Keppler, *Inorg. Chem.*, 2005, **44**, 6704-6716.
9. K. R. Brown, G. L. Keller, I. J. Pickering, H. H. Harris, G. N. George and D. R. Winge, *Biochemistry*, 2002, **41**, 6469-6476.